

Low-Energy Electron Diffraction With Energy Invariant Carrier Wave Wavenumber Modulated by Exchange-Correlation Interaction

John Rundgren,^{1,*} Wolfgang Moritz,^{2,†} and Bo E. Sernelius^{3,‡}

¹*Department of Physics, KTH Royal Institute of Technology, 10691 Stockholm, Sweden*

²*Department of Earth and Environmental Sciences, Ludwig-Maximilians-University, Theresienstrasse 41, 80333 Munich, Germany*

³*Department of Physics, Chemistry and Biology, Linköping University, 58183 Linköping, Sweden*

(Dated: October 21, 2020)

We present low-energy electron diffraction (LEED) as elastic electron-atom scattering (EEAS) operating in a target crystal waveguide where a Coulombic carrier wave is wavelength modulated by exchange-correlation (XC) interaction. Carrier potential is designed using a KKR (Korringa-Kohn-Rostoker) muffin-tin model built on overlapping free atoms. XC potential is constructed using Sernelius's multiple-particle theory on electron self-energy. Dirac's differential equations are solved and EEAS phase shifts are calculated. Their qualifications are tested by recalculation of four recent LEED investigations. We are able to report substantially improved reliability factors.

A common effort in surface structure investigations by LEED (low-energy electron diffraction) is to measure interatomic distances reliably with 0.001 nm precision. LEED experience shows that the precision is limited by the elastic electron-atom scattering (EEAS) phase shifts injected as input to the diffraction codes.[1–3] In a new study of EEAS we set up a KKR (Korringa-Kohn-Rostoker) muffin-tin (MT) potential with overlapping MT spheres corresponding to N_{ieq} symmetrically inequivalent atoms in the surface structure. It is clear that N_{ieq} radial overlaps give rise to $2N_{\text{ieq}}$ degrees of freedom due to overlapping MT sphere radii and possible energy shifts of atomic potentials. In contrast, the KKR approach of Mattheiss [4–6] fixes each touching atom potential on the energy axis by superposition of neighbor potential tails, making N_{ieq} atomic energy shifts inaccessible to crystalline optimization. Advantage overlapping MT spheres. The plan of the present work is, first, to design N_{ieq} MT overlap parameters S_i , second, to build a coherent crystal potential from N_{ieq} atomic potentials, and, thereafter, to perform LEED structure investigation by adjusting overlap potentials to least possible Pendry reliability factor.[7]

We are going to describe EEAS with similar terminology as used for electromagnetic scattering like teletransmission and radar, with concepts waveguide, carrier wave, and modulation by frequency or wavenumber. The target crystal is naturally a wave guide. A low-energy incident electron exerts spin and charge repulsion about herself, weakening local nuclear screening. Resulting additional nuclear attraction contributes negative self-energy Σ that scatters the signal electron by her own exchange (X) -correlation (C) potential. In transmission electron microscopy (TEM, 200 keV–1 MeV) the signal electron traverses the crystal with speed making the crystal's electron and nuclear interactions seem frozen due to the finite relaxation time of the electron gas. Correspondingly, the self-energy tapers off to nothing when crystal's electron gas approaches ground state. A pure high-energy sig-

nal is guided by an electrostatic mass-and-charge atomic potential, Coulombic and energy invariant that acts as signal carrier wave at all energies above Pauli indistinguishability limit ~ 10 eV. With increasing incidence E the self-energy runs through a minimum about the plasmon threshold ~ -10 eV at $E \sim 20$ eV; with increase to very high E the self-energy asymptotically approaches zero and gets negligible. The XC potential adds to the carrier potential and gives rise to wavenumber modulation of the carrier wave.

The paper continues with the following paragraphs: The design of a KKR overlap MT model and the construction of the corresponding carrier potential; the construction of an XC modulation potential using Sernelius's data base on signal electron self-energy; the integration of Dirac's differential equations with modulated carrier potential; and, in the interstice, the reduction of the first-order Dirac equations into a second-order Schrödinger equation exhibiting a relativistic energy-dependent XC potential. Finally, EEAS phase shifts are calculated, the qualifications of which we successfully test by recalculating four published LEED investigations.[8–11]

We initiate the EEAS theory by constructing the carrier potential. The surface unit cell of the crystal is supposed to contain N_{ieq} inequivalent atom types $i = 1, 2, \dots, N_{\text{ieq}}$, where each index i corresponds to a subset of $N_{\text{eq}i}$ symmetrically equivalent atoms; N_{uc} is total number of atoms in the unit cell. Assigned to each site i is an atom of electron density $\rho_i(r)$ and nucleus Z_i . We utilize computer code available from National Institute of Science and Technology [12, 13] for calculating Coulombic potentials $V_{\text{NIST}i}(r)$ from $\rho_i(r)$ and Z_i by Poisson integration with standard normalization, potential tending to zero at large radius. Given $V_{\text{NIST}i}(r)$, we wish to build a KKR crystal carrier potential $V_i(r)$, $r \leq R_i$, $i = 1, 2, \dots, N_{\text{ieq}}$, where R_i signifies MT radius. A crucial point in the modeling of a carrier potential is that potential level $V_{\text{NIST}i}(R_i)$ is arbitrary with respect to the searched crystalline potential level $V_i(R_i)$. Differ-

ential evolution (DE) [14] is an appropriate method for extracting information from an EEAS picture with $2N_{\text{ieq}}$ degrees of freedom. Considering the framework of symmetrically inequivalent atoms, we pay particular attention to two overlapping MT spheres of radii R_i and $R_{\text{NN}i}$ positioned at interatomic distance endpoints, subscript $\text{NN}i$ signifying next neighbor of atom i . Quantitatively we define the MT spheres overlap by the inequality

$$R_i + R_{\text{NN}i} \leq d_{i,\text{NN}i} \times (1 + S_i), \quad i = 1, 2, \dots, N_{\text{ieq}} \quad (1)$$

where $d_{i,\text{NN}i}$ is interatomic distance, and overlap parameter S_i indicates relative overlap with respect to touching spheres. Supposing that MT radii R_i are known, we set up a spatially constant interstitial potential V_0 equal to the unit cell average of the atomic potentials at MT sphere peripheries,

$$V_0 = N_{\text{uc}}^{-1} \sum_{i=1}^{N_{\text{ieq}}} N_{\text{eq}i} V_i(R_i) \quad (2)$$

Here, a signal electron scattering argument comes in. Signal electron reflection at potential steps between interstitial V_0 and peripheral $V_i(R_i)$ would excite alien standing-wave resonances in the MT spheres. Removal of potential steps is thus found to be a necessary condition on clean signal electron EEAS in the crystal. The requirement corresponds to a DE fitness number based on the N_{ieq} degrees of freedom in potential formation,

$$\epsilon = \min \left[\max_i (|V_i(R_i) - V_0|) \right], \quad i = 1, 2, \dots, N_{\text{ieq}} \quad (3)$$

The application of DE on equations (1)–(3) starts from the work space $V_i(r) = V_{\text{NIST}i}(r)$, $i = 1, 2, \dots, N_{\text{ieq}}$. A first DE calculation creates sets R_i and $V_i(r)$ with a coarse fitness number $\epsilon = O(1)$ in units of eV. Preparatory to a continued DE calculation we make the following substitution,

$$V_i(r) - [V_i(R_i) - V_0] \rightarrow V_i(r), \quad i = 1, 2, \dots, N_{\text{ieq}} \quad (4)$$

noting that V_0 remains invariant. With one more turn DE finishes with $\epsilon = O(10^{-15})$ in a computer of 64 bit precision. So far our KKR-MT model is solved exactly. However, the energy level of V_0 is undefined until we connect the surface slab unit cell to the crystal bulk. Fortunately, a slab-to-bulk boundary condition is inherent in the DE method. We force the MT radii of the innermost layers of the surface unit cell to optimize in minute intervals prepared to contain known MT radii of the bulk; in this way DE optimization lifts V_0 to bulk energy level. In next paragraph we learn that electron self-energy is currently normalized to zero at infinite incident energy. Correspondingly, a consistent total crystal potential is created using an energy invariant carrier potential $V_i(r)$, $i = 1, 2, \dots, N_{\text{ieq}}$ normalized to $V_0 = \text{MTZ}$ (muffin-tin zero) = 0.

Rayleigh-Schrödinger (RS) multiple-particle physics theory[15] describes the signal electron as a one-electron

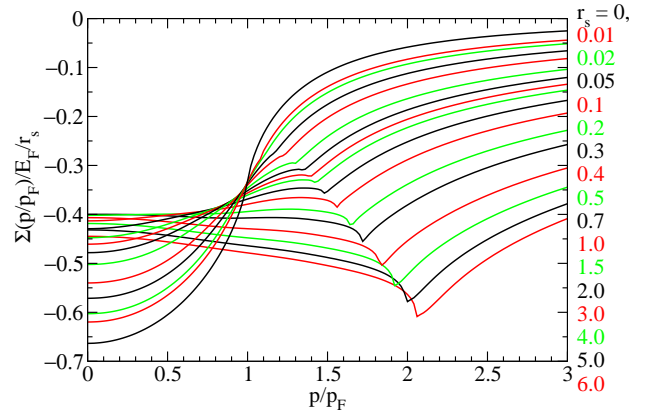


FIG. 1. XC interaction as function of signal electron momentum p and interelectronic spacing r_s in target electron gas.

excitation of the crystal electron gas. The excitation gives rise to a kinetic energy contribution accelerating the signal electron and a nuclei induced self-energy contribution adding a piece of XC potential to the carrier wave. The multi-particle picture of signal electron scattering is illustrated by equation (5) showing the energy balance between the one-electron excitation acting as signal electron in the left-hand member and an energy reservoir of incident energy and crystal ground-state chemical potential in the right-hand member,[16–18]

$$p(r_s)^2 + \Sigma[p(r_s), r_s] = E + E_F(r_s) + \Sigma[p_F(r_s), r_s] \quad (5)$$

Designations are: p = signal electron momentum, equal to wavenumber in atomic Rydberg units, Σ = signal electron self-energy, p_F = Fermi momentum, E_F = Fermi energy, and r_s = electron-space radius expressing electron gas density ρ , $(4\pi/3)r_s^3\rho = 1$. Electron space r_s measuring 0–6 in units of Bohr radius covers most crystals. Using RS perturbation theory Sernelius worked out a data base for the self-energy,[18]

$$\text{sdat}(p/p_F, r_s) = \Sigma(p/p_F)/(E_F r_s) \quad (6)$$

with p/p_F running from 0 to 3 and r_s in Bohr units from 0 to 6. Figure 1 shows sdat in diagram form. For momentum exterior to the diagram, Σ is continued by extrapolation to Lindhard's correlation potential $-(\pi^3\rho)^{1/2}/p$, nonconverging with p but considered negligible at TEM energy,[19] together with Hartree-Fock exchange potential vanishing as $-2\pi\rho/p^2$. [20] Equation (5) is solved with respect to relative momentum p/p_F using data base sdat with bivariate interpolation,[21]

$$(p/p_F)^2 = (E/E_F) + 1 + r_s[\text{sdat}(1, r_s) - \text{sdat}(p/p_F, r_s)] \quad (7)$$

The result is expressed in terms of atomic XC potentials

$$V_{\text{XC}i}(r, E) = \text{sdat}(p/p_F, r_s) E_F r_s, \quad i = 1, 2, \dots, N_{\text{ieq}} \quad (8)$$

where r and r_s share the same radial point grid. A fitness factor f_{XC} is multiplied into the right-hand member of

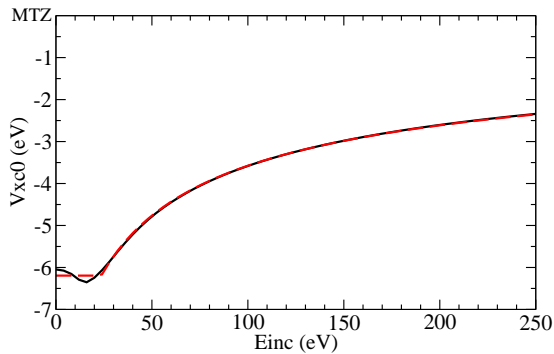


FIG. 2. Interstitial XC potential (black) and a four-coefficient approximation (red) for Cu(111)+(3 $\sqrt{3} \times \sqrt{3}$)R30 $^\circ$ -TMB. $V_{XC0} = \text{MTZ}$ is energy level of vanishing electron self-energy.

eq. (8) for the purpose of a tentative theory–experiment study of **sdat**. We set up a spatially flat inner XC potential to eliminate alien scattering in MT spheres,

$$V_{XC0}(E) = N_{uc}^{-1} \sum_{i=1}^{N_{ieq}} N_{eqi} V_{XCi}(R_i, E) \quad (9)$$

Substitution similar to (4) renormalizes the atomic XC potentials to no steps, $V_{XCi}(R_i, E) = V_{XC0}(E)$, approaching MTZ at very high E . The $V_{XC0}(E)$ versus E curve turns out to have universal shape given by a four-coefficient approximation,[19, 22]

$$V_{XC0}(E) \approx \max [c_1 + c_2/\sqrt{E + c_3}, c_4] \quad (10)$$

whose increasing part almost identically fits the calculated XC potential. See Fig. 2.

Relativistic EEAS with central potential is determined by Dirac equation $W\psi = H\psi$, where ψ is two-component spinor.[23] Hamiltonian eigenstates are $G_\kappa = u_{1\kappa}/r$ and $F_\kappa = u_{2\kappa}/r$ corresponding to energy eigenvalue $W = E + \frac{1}{2}c^2$, where $\frac{1}{2}c^2$ is the relativistic rest-mass energy in atomic Rydberg units. Speed of light $c = 274.073$ is twice the fine-structure constant. $u_{1\kappa}$ and $u_{2\kappa}$ are solutions of two Dirac differential equations with central potential,

$$\begin{aligned} \frac{du_{1\kappa}}{dr} &= -\frac{\kappa}{r}u_{1\kappa} + \{c + c^{-1}[E - V_{Ti}(r, E)]\}u_{2\kappa} \\ \frac{du_{2\kappa}}{dr} &= \frac{\kappa}{r}u_{2\kappa} - c^{-1}[E - V_{Ti}(r, E)]u_{1\kappa} \end{aligned} \quad (11)$$

where $V_{Ti}(r, E)$ signifies total potential per atom equal to $V_i(r) + V_{XCi}(r, E)$. κ is spin-orbit quantum number, j total angular momentum, and l atomic orbital,

$$\kappa = \begin{cases} -l - 1 & \text{for } j = l + \frac{1}{2}, l = 0, 1, 2, \dots \\ l & \text{for } j = l - \frac{1}{2}, l = 1, 2, \dots \end{cases} \quad (12)$$

κ is negative or positive corresponding to spin $\frac{1}{2}$ parallel or $-\frac{1}{2}$ antiparallel to electron's direction of flight. A single s wave of spin $\frac{1}{2}$ is transmitted in forward direction. In the signal electron wave field $u_{1\kappa}$ is referred to as the

TABLE I. Comparison of reliability factors obtained from phase shifts with MT potentials using touching (T) and overlapping (O) spheres. MT overlap $S = 0.3 - 0.4$ and self-energy factor $f_{XC} = 1.0$.

Surface structure	energy (eV)	reliability	
		T	O ^a
Ag(111)+(7 \times $\sqrt{3}$)rect-SO ₄	10-150	0.235 ^b	0.21
Cu(111)+(3 $\sqrt{3} \times \sqrt{3}$)R30 $^\circ$ -TMB	11-200	0.32 ^c	0.26
Ru(0001)+($\sqrt{3} \times \sqrt{3}$)R30 $^\circ$ -Cl	20-300	0.137 ^d	0.11
Ag(111)+(4 \times 4)-O	25-250	0.34 ^e	0.29

^aThis work. ^bRef.[8]. ^cRef.[9]. ^dRef.[10]. ^eRef.[11].

large Dirac spinor having by a factor of c greater amplitude than $u_{2\kappa}$. Integration starts at $r = 0$ from boundary conditions

$$u_{1\kappa} = Ar^\gamma \quad \text{and} \quad u_{2\kappa} = Ar^\gamma(\kappa + \gamma)/\zeta \quad (13)$$

with $A = \text{const}$, $\gamma^2 = \kappa^2 - \zeta^2$, $\zeta = e^2Z$, and $Z =$ atomic number. Integration of eqs. (11) is numerically feasible with the given γ at $l = 0$ but turns impracticable with increasing l , when angular momentum displaces the start of wave functions to greater radii. With $l \geq 1$ we start integration at exponential grid point r_n with $(r_n)^{|\gamma|} = r_1$. The Dirac equations are integrated by means of Shampine and Gordon's ODE (ordinary differential equation) solver built on Adams predictor-corrector method with automatic initiation and step size control.[24]

In the interstice of spatially constant potential V_{XC0} , the wave field is well described by elimination of $u_{2\kappa}$ from the first-order differential equations (11), $u_{2\kappa}$ having relative magnitude c^{-1} . The carrier cancels out, and we get a second-order Schrödinger equation for $u_{1\kappa}$ in XC space,

$$\begin{aligned} \frac{d^2u_{1\kappa}}{dr^2} + \left[q^2 - \frac{\kappa(\kappa + 1)}{r^2} \right] u_{1\kappa} &= 0 \\ q^2 = E - V_{XC0}(E) + c^{-2}[E - V_{XC0}(E)]^2 \end{aligned} \quad (14)$$

The difference between wavenumbers q and \sqrt{E} expresses the XC modulation of the carrier wave (atomic Rydberg units). $\kappa(\kappa + 1)$ equals $l(l + 1)$ for both spins, and the eigenvectors are $rj_l(qr)$ and $ry_l(qr)$ with spherical Bessel functions j_l and y_l . The signal electron in the interstice is expressed in terms of scattering phase shifts δ_κ ,

$$u_{1\kappa}(r) = C[rj_l(qr) \cos \delta_\kappa - ry_l(qr) \sin \delta_\kappa] \quad (15)$$

$C = \text{const}$. κ takes a single subscript -1 for orbital $l = 0$ and otherwise two subscripts, $-l - 1$ and l , for orbitals $l \geq 1$. The phase shifts δ_κ are determined by equating logarithmic derivatives belonging to wave functions inside and outside MT radius R . With prime for differentiation with respect to r , phase shifts are obtained from

$$\tan \delta_\kappa = \frac{[u_{1\kappa}(r)]' r j_l(qr) - u_{1\kappa}(r) [r j_l(qr)]'}{[u_{1\kappa}(r)]' r y_l(qr) - u_{1\kappa}(r) [r y_l(qr)]'} \Big|_{r=R_i} \quad (16)$$

The phase shift spin states define two sets of scattering amplitudes, $q^{-1}e^{i\delta_{-l-1}} \sin \delta_{-l-1}$ and $q^{-1}e^{i\delta_l} \sin \delta_l$, of spin $\frac{1}{2}$ and $-\frac{1}{2}$, respectively. In the LEEDFIT code [25] these quantities are composed to Schrödinger scattering amplitudes with relative orbital factors $l+1$ and l . LEEDFIT optimizes atomic positions in the structure by performing electron diffraction, producing theoretical spectra, and controlling their agreement with experiment by means of reliability factor minimization.[7] Phase shifts δ_κ are iteratively applied in internal loops on atomic position variation; new positions require new phase shifts. At the same time δ_κ 's participate in external theoretical variations on overlap parameters S_i and self-energy factor f_{XC} . An EEAS code for δ_κ is incorporated as a kernel in LEEDFIT.

Table I is a quality mark on the present work. Four recently determined LEED structures are reinvestigated, and we conclude that full utilization of $2N_{ieq}$ degrees of freedom in the KKR overlap MT atom model give rise to significantly improved reliability factors relative to earlier Mattheiss KKR recipes. Secondly, a gratifying observation from the LEED studies in Table I is that the factor f_{XC} on XC interaction equals unity. We conclude that Sernelius's self-energy data are perfectly valid for LEED – provided electron surface barrier transmission is closely unity between target crystal and electron recorder in vacuum. Thirdly, we find from the aforementioned structures that an initially supposed set of atomic overlap parameters S_i is replaceable by a single structural parameter S . In Table I S takes values in the span $0.3 - 0.4$.

In summary, our report introduces new EEAS concepts in LEED: target wave guide, carrier wave, and modulation by self-energy. We show that the carrier potential is identical to the electron scattering potential in TEM and therefore Coulombic and energy invariant. The consequence is that the carrier potential and the XC potential are decoupled, having none and active energy dependence, respectively. In the interstice the total potential has XC energy profile, observed as wavenumber modulation on the carrier potential and wave. This verifies the similar scattering pictures of EEAS in crystal and electromagnetic beam transmission in atmosphere.

Financial supports from KTH Royal Institute of Technology, Ludwig-Maximilians-University, and Linköping University are gratefully acknowledged.

* jru@kth.se

- † wolfgang.moritz@lrz.uni-muenchen.de
 ‡ bo.e.sernelius@liu.se
- [1] D. K. Saldin and J. C. H. Spence, *Ultramicroscopy* **55**, 397 (1994).
 - [2] S. Walter, V. Blum, L. Hammer, S. Müller, K. Heinz, and M. Giesen, *Surf. Sci* **458**, 155 (2000).
 - [3] J. Vuorinen, K. Pussi, R. D. Diehl, and M. Lindroos, *J. Phys. Condens. Matter* **24**, 015003 (2012).
 - [4] L. F. Mattheiss, *Phys. Rev.* **133**, 184 (1964).
 - [5] T. Loucks, *Augmented Plane Wave Method* (Benjamin, New York, 1967).
 - [6] A. Barbieri and M. A. VanHove, *Phase Shift Package* (2007), www.icts.hkbu.edu.hk/vanhove/VanHove_files/phshift2007.zip.
 - [7] J. B. Pendry, *J. Phys. C* **13**, 937 (1980).
 - [8] R. Wyrwich, T. E. Jones, S. Günther, W. Moritz, M. Ehrensperger, S. Böcklein, P. Zeller, A. Lünser, A. Locatelli, T. O. Mentès, M. A. Niño, A. Knop-Gericke, R. Schlögl, S. Piccinin, and J. Wintterlin, *J. Phys. Chem. C* **122**, 26998 (2018).
 - [9] T. Sirtl, J. Jelic, J. Meyer, K. Das, W. Heckl, W. Moritz, J. Rundgren, M. Schmittel, K. Reuter, and M. Lackinger, *Phys. Chem. Chem. Phys.* **15**, 11054 (2013).
 - [10] J. P. Hofmann, S. F. Rohrlack, F. Hess, J. C. Goritzka, P. P. T. Krause, A. P. Seitsonen, W. Moritz, and H. Over, *Surf. Sci.* **606**, 297 (2012).
 - [11] R. Reichelt, S. Günther, J. Wintterlin, W. Moritz, L. Aballeb, and T. O. Mentès, *J. Chem. Phys.* **127**, 134706 (2007).
 - [12] E. L. Shirley, *Hartree-Fock program* (1995), eric.shirley@nist.gov.
 - [13] S. Kotochigova, Z. H. Levine, E. L. Shirley, M. D. Stiles, and C. W. Clark, *Phys. Rev. A* **55**, 191 (1997).
 - [14] R. Storn and K. Price, *J. Global Opt.* **11**, 341 (1997), <http://www.icsi.berkeley.edu/~storn/code.html>.
 - [15] G. D. Mahan, *Many-Particle Physics*, 3rd ed. (Kluwer Academic/Plenum Press, New York, 2000).
 - [16] L. Hedin and B. I. Lundqvist, *J. Phys. C* **4**, 2064 (1971).
 - [17] R. E. Watson, J. F. Herbst, L. Hodges, B. I. Lundqvist, and J. W. Wilkins, *Phys. Rev. B* **13**, 1463 (1976).
 - [18] K. W. K. Shung, B. E. Sernelius, and G. D. Mahan, *Phys. Rev. B* **36**, 4499 (1987).
 - [19] J. Lindhard, *Kgl. Danske Videnskab. Selskab. Mat.-Fys. Medd.* **28**, No. 8 (1954), p. 47.
 - [20] N. W. Ashcroft and N. D. Mermin, *Solid State Physics* (Saunders College, Philadelphia, 1976).
 - [21] Ref. ? : Sec. 25.2.66.
 - [22] J. Rundgren, *Phys. Rev. B* **68**, 125405 (2003).
 - [23] M. E. Rose, *Relativistic Electron Theory* (Wiley, New York, 1961).
 - [24] L. F. Shampine and M. K. Gordon, *Computer Solutions of Ordinary Differential Equations* (1975), <http://www.netlib.org/>.
 - [25] W. Moritz and M. A. VanHove, *Surface Structure Determination by LEED and X-rays*, (to be published).